

# Design and Analysis of Equipment for Load Introduction during Full Scale Blade Test

J. K. W. Andersen, M. B. Escudero, L. H. Larsen, J. Thuesen and A. Vissamsetty

Department of Materials and Production, Aalborg University  
Fibigerstraede 16, DK-9220 Aalborg East, Denmark

Email: [jkwa17](mailto:jkwa17@student.aau.dk), [mberme20](mailto:mberme20@student.aau.dk), [lhla17](mailto:lhla17@student.aau.dk), [jthues17](mailto:jthues17@student.aau.dk) & [avissa20](mailto:avissa20@student.aau.dk) @student.aau.dk,

Web page: <http://www.mechman.mp.aau.dk/>

## Abstract

Full scale blade testing is an important part of the validation process in the design of a wind turbine blade. As demands for more efficient turbine blades is ever increasing, testing methods need to be improved and understood better. The tests need to be as realistic as possible, so that the margin of safety can be minimised. Currently, the static tests are performed by applying loads at different points along the length of the blade. The loads are introduced by clamping the blade with steel yokes and wooden inserts that follow the profile of the blade. This generates some undesirable local effects around the points of the load introduction, such as stiffening of the blade in the span-wise direction and stress concentrations. The goal of this project is to study the local effects of the load introduction and to devise a method that minimizes such effects. This project is done in collaboration Siemens Gamesa Renewable Energy.

**Keywords:** Wind turbine blades, Load introduction, Static test, Composite structure, Finite elements

## 1. General introduction

Nowadays, global warming and limited energy resources are several of the world's problems. Therefore, clean energy, as wind energy, is a good alternative. The main components of a Horizontal Axis Wind Turbine (HAWT) are shown in Figure 1 and the purpose of the wind turbine is to harvest the kinetic energy from the wind and turn it into electric energy. This is done by spinning the rotor which turns an electric generator.

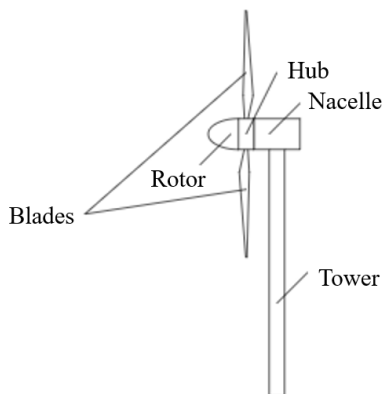


**Fig. 1** Main components of a HAWT.

The typical cross section of a turbine blade is illustrated in Figure 2. The shell is good at resisting torsional loads and edgewise bending while the shear stresses are

carried by the shear web, which connects the pressure and suction side [1].

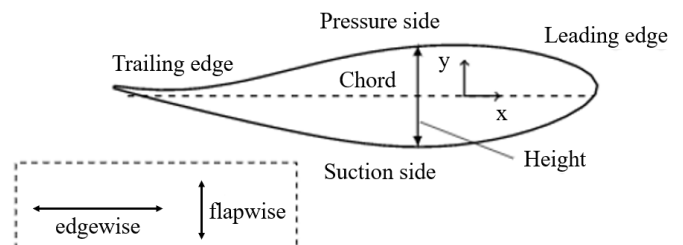


**Fig. 2** Main terms of an airfoil.

According to [2], the design of a wind turbine blade is always a compromise between aerodynamics, structural integrity, costs and manufacturing. This compromise is achieved through an iterative process, where an optimum between structural integrity and aerodynamic efficiency is achieved. Due to the importance of the blade and its structural integrity, several load introductions during full scale blade tests are carried out to verify the reliability of the computational design model and to assess the load carrying capacity [3].

### 1.1 Testing of blades

In order to verify the structural integrity of the blade SGRE performs different full scale tests to emulate the real-life behaviour. These full scale tests consist of a

initial static test, followed by a dynamic test and finally a static test again.

The goal with the static test, is to pretend a strong gust of wind impacting on the blade. The tests are performed by adding loads to the blade and carrying out several tests in four directions, see Figure 3.

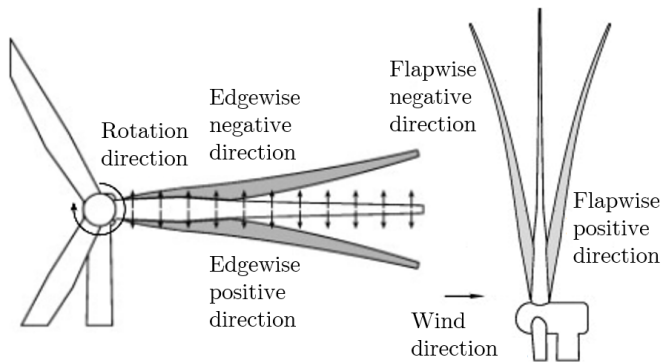


**Fig. 3** Loading directions [4] (modified).

In order to approximate the real moment distribution, the blade is loaded by shear forces at different places along the blade span.

The method used is the the multi-point method, where the blade is loaded at different points along the blade at the same time.

The load is introduced using yokes which are wooden structures that are clamped around the blade. These yokes are assumed to stiffen the blade around the yoke which, in addition to the local load introduction, causes the blade to behave differently around the yokes. Therefore, the results within  $\pm 75\%$  of the chord length, in the spanwise direction, are considered invalid [5]. However, SGRE has not fully investigated these local effect.

A better understanding of the local effects and how these can be reduced will therefore lead to better test methods which further might lead to better blades and thus reduce costs in the long term.

## 2. Materials and methods

### 2.1 Data from Siemens Gamesa Renewable Energy

This project was carried out in collaboration with SGRE. The company providing a FEM shell model of a 112 m long blade with material data defined, selective strength data, moment curves and a CAD-drawing of a yoke.

The coordinate system in Figure 4 is used throughout the article to describe the shell model. The shell model

consisted of 13 different materials which together made up the entire blade. In the FEM shell model, there were two different element types defined, SHELL181 and SOLID187. The shell elements were used to describe the outer shell, the shear web and the mini web, while the solids described the trailing edge reinforcement, as shown in Figure 5.

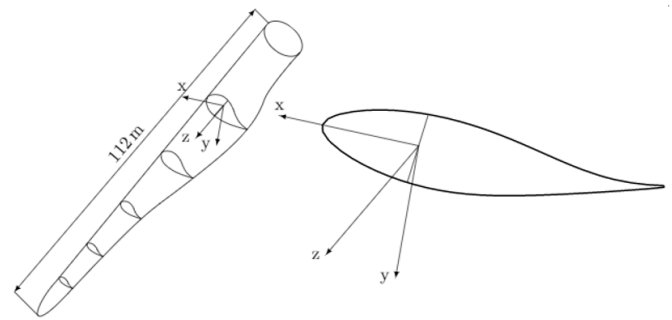


**Fig. 4** Tool Coordinate System of the blade from SGRE.

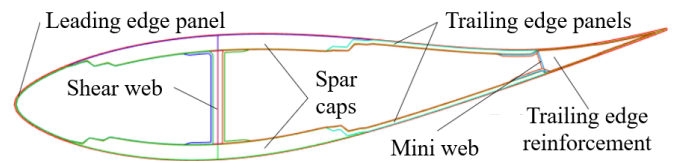


**Fig. 5** Tool Coordinate System of the blade from SGRE.

For the shell elements distinct sections were defined, related to the layup. The number of layers depended on the part of the blade, and they went from 1 to 13 layers. All of them were at zero degrees and the sections attached to the outer shell were offset to the top-plane while the two webs were mid offset.

The spar caps were made of unidirectional carbon and glass fibers as well as biax glass fibers. The shear web and the mini web of biax glass fiber. The leading and trailing edge panel were sandwich structures consisting of a combination of unidirectional glass fiber, biax glass fiber and some balsa wood as core material. Pur foam was used for the trailing edge reinforcement.

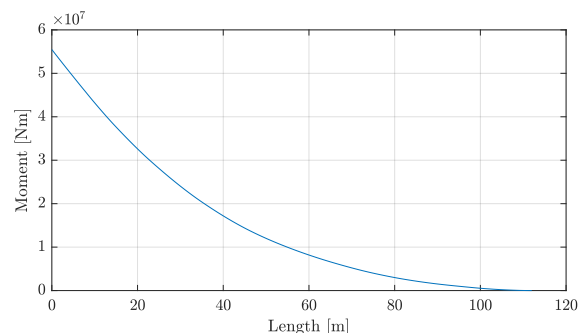


**Fig. 6** SGRE moment load for flapwise positive.

The moment load along the blade is illustrated in Figure 6 for the flapwise positive direction. Similar plots for the three remaining load directions were also provided. However, the focus of this article was only on the flapwise positive direction.

## 2.2 Ideal loading of blade

### 2.2.1 Modelling ideal boundary conditions

The modelling choices which were made to model an ideal loading of the wind turbine blade were based on the moment curves provided by SGRE. This ideal load case was used as a reference model for the other FEM-analysis, so that the local effects introduced by the yokes could be investigated.

The load acting on the blade in this ideal load case was divided into two different parts, a gravitational load and the remaining load, referenced as the ideal test load. The gravitational load was applied as a body force in the FEM-analysis, while the test load was distributed by applying shear forces along the nodes that connect the shear web and the spar caps. The boundary conditions for this ideal model are illustrated in Figure 7.

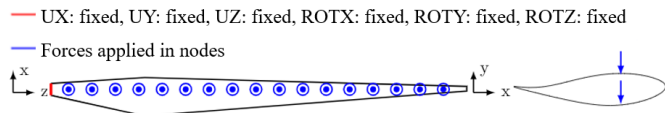


**Fig. 7** Boundary condition used for modelling the ideal load case.

The ideal test load was obtained by first determining the loads in the nodes along the shear web, which when applied would yield a moment curve along the blade almost equivalent to the SGRE moment curve. This moment curve is referenced as the approximate moment curve. Afterwards the gravity load was subtracted to obtain the ideal loads.

The loads in the node which yielded a moment curve almost equivalent to the SGRE moment curve were found by fitting a B-spline through the SGRE moment curve and differentiating it twice to obtain the load distribution. Different B-splines were fitted to the SGRE moment curve by use of a least-squares B-spline approximation in MATLAB. The best B-spline fit was found based on the residual between the approximate moment curve and SGRE moment curve and a manual judgment of the load distribution. The load distribution along the blade for the ideal test load is illustrated in Figure 8.

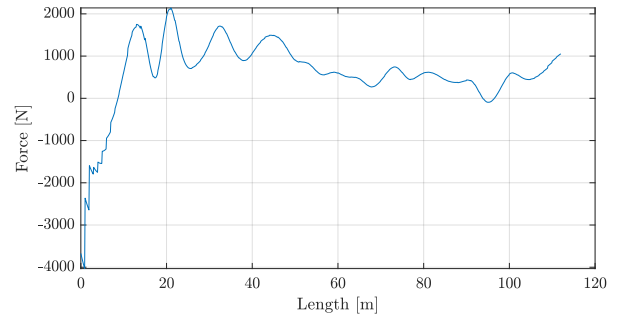


**Fig. 8** Load distribution for flapwise positive with and without gravity.

### 2.2.2 Linear vs. non linear analysis

Depending on the load case investigated, the vector sum of the tip displacement was in the range of 9-30 m for a linear analysis. Therefore, large deformations have to be taken into account when modelling the blade, and the linear analysis does not consider them. Therefore, a nonlinear geometric analysis was performed to account for stiffness changes. In addition, this analysis uses the equations of equilibrium in the deformed geometry.

To investigate the effect of including non linearity in the model, a linear and a nonlinear analysis was performed and compared. However, during the nonlinear modelling of the blade several problems were encountered. First, only the two flapwise load cases succeeded in converging to a solution. Secondly, during the post processing of the nonlinear modelling of the blade in the flapwise direction, buckling was experienced in the shear web for the negative direction and in the trailing edge panels for the positive direction.

Hence, a linear eigenvalue buckling analysis was performed to get an estimation of the buckling load and the modes. The first buckling mode shape is evident from Figure 9a. The corresponding buckling load multiplier is 0.73, which means that the load applied in the model is above the critical buckling load. Figure 9b. illustrates the trailing edge panel, for the same cross section, but from a geometrical nonlinear buckling analysis.

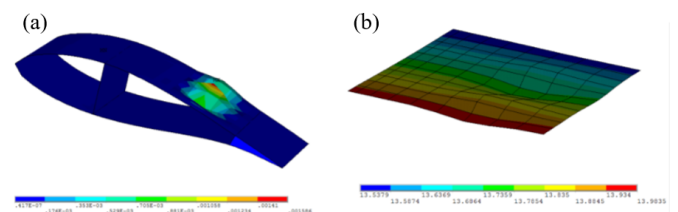


**Fig. 9** (a) First buckling mode from linear buckling analysis. (b) Buckling from geometrically non-linear buckling analysis.

Due to the fact that the model was supplied by SGRE, it was not straight forward to make any modifications to the blade. As this buckling behaviour is an inherent defect in the model, only linear analysis of the blade was done.

### 2.3 Yoke placement

As local effects from the yokes were evident, it was desirable to have as few yokes as possible placed on the blade while approximating the design moment curve as close as possible during a test, without making the blade fail. In order to determine the best yoke position, the SGRE moment curve in Figure 6 was divided into a gravitational moment and a ideal test load moment, equivalent to the method described in subsection 2.2. This ideal test load moment is plotted in Figure 10 and it is this moment curve which should be approximate by applying shear forces in the yokes.

The moment curve resulting from applying shear forces in the yokes are referred to as the *yoke moment curve*. The yoke moment curve is also evident from Figure 10. The yoke moment curve is a piecewise linear curve and the change in slope between each individual linear part of yoke moment curve defines the loads, to apply at each yoke point.

The placement of the yokes was based on the optimization problem defined in Equation 1-3b. This optimization problem had the yoke position,  $x_j$ , along the blade as the design variables and tried to minimize the residual between the ideal test moment and the yoke moment curve, by placing the yokes in the best possible position. The residual was evaluated for every half meter. This was done in the inner summation in Equation 1. The outer summation in Equation 1 sums the sum of residuals for all four load cases. This was done such that the best possible compromise for the yoke positions, when considering all four load directions, was found. Thereby, it was only necessary to position the yoke once in order to be able to test in all directions.

The objective chosen was the minimization of the largest residual, but since this would yield in a non-continuous problem, it was implemented by the use of a p-norm function where the residuals were raised to the power of 6. All the variables in the optimization problem are defined in the list below.

- $x_j$  are the design variables in the optimization problem.

- $\bar{x}_i$  are the the evaluation points wherein the residual is evaluated.
- $\bar{y}_m(\bar{x}_i)$  is the correct moment curve value at evaluation point  $\bar{x}_i$  for load case  $m$ .
- $y_{app,m}(x_j, \bar{x}_i)$  is the approximate moment curve value in evaluation point  $\bar{x}_i$ . The approximate moment curve is also dependent on the design variables  $x_j$ .
- $\bar{y}_m(x_j)$  is the correct moment curve value evaluated in the yoke points.

$$f(\mathbf{x}) = \sum_{m=1}^4 \left( \sum_{i=1}^{225} (\bar{y}_m(\bar{x}_i) - y_{app,m}(x_j, \bar{x}_i))^6 \right)^{\frac{1}{6}} \quad (1)$$

$$y_{app,m}(x_j, \bar{x}_i) = \begin{cases} a_1 \bar{x}_i + b_1 & 0 < \bar{x}_i \leq x_1 \\ a_2 \bar{x}_i + b_2 & x_1 < \bar{x}_i \leq x_2 \\ \vdots & \\ a_j \bar{x}_i + b_j & x_{j-1} < \bar{x}_i \leq x_j \\ \vdots & \\ a_n \bar{x}_i + b_n & x_{n-1} < \bar{x}_i \leq x_n \end{cases} \quad (2)$$

$$a_j(x_j) = \frac{\bar{y}_m(x_j) - \bar{y}_m(x_{j-1})}{x_j - x_{j-1}} \quad (3a)$$

$$b_j(x_j) = \bar{y}_m(x_j) - a_j x_j \quad (3b)$$

Additionally, three constraints were included in the optimization problem. The first constraint in Equation 4a ensured that the yoke was placed within acceptable limits on the blade. The second constraint ensured that the yokes were spaced at least one meter apart. The last constraint in Equation 4c was imposed as the current test set up used by SGRE only allows the force to be applied in a downward direction.

$$0 \leq x_j \leq 110 \quad (4a)$$

$$x_{j-1} + 1 < x_j \quad (4b)$$

$$a_{j-1} > a_j \quad (4c)$$

The optimization problem was solved eight times with the number of yokes varying from 1 to 8. Based on the sum of residual for each solved optimization problem, 5 yokes were deemed the best solution. The yoke position and the forces to be applied in each yoke point are listed in Table I.

Design variable	$x_1$	$x_2$	$x_3$	$x_4$	$x_5$
Yoke position [m]	16.6	31.3	57.4	94	110
Edgewise neg. [kN]	251.6	372.8	31.2	0	126.3
Edgewise pos. [kN]	246.2	394.2	0	24.3	116
Flapwise neg. [kN]	0	133.0	318.9	275.2	73.8
Flapwise pos. [kN]	121.2	224.5	201.5	92.2	58.8

**Tab. I** Final yoke position, which yields the best possible approximate moment curve.

For the yoke points wherein the force was zero, it was necessary to remove the yoke before the test, due to the weight of the yoke.

The approximate moment curve for the flapwise positive load case is plotted on top of the correct moment curve in Figure 10. Furthermore, the magnitude of the residual between the approximate and correct moment curve is illustrated.

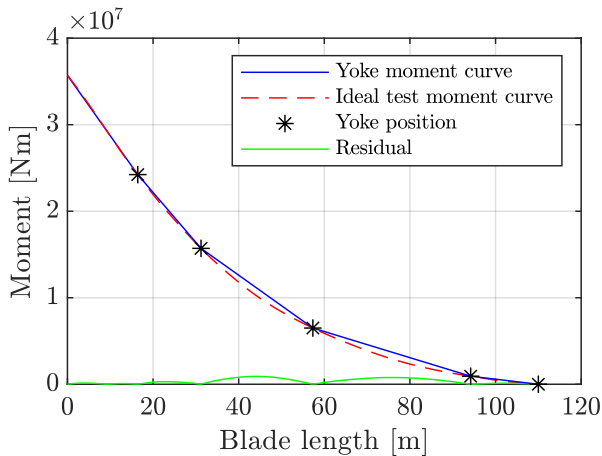


**Fig. 10** Yoke and ideal test moment curves for the flapwise positive load cases. Also the yoke positions are illustrated.

### 2.3.1 Simple yoke modelling

First, a simple model of the blade loaded in the yoke points was built. This model worked as an initial model for the yokes and as a model, which could be build upon in order to later set up a more accurate and complex model.

To simulate actual load conditions, the pressure was distributed, on the suction side for the load case considered. Additionally, the gravitational load was applied as a body force. The blade was fixed at the root and all the boundary conditions in the model are shown in Figure 11.

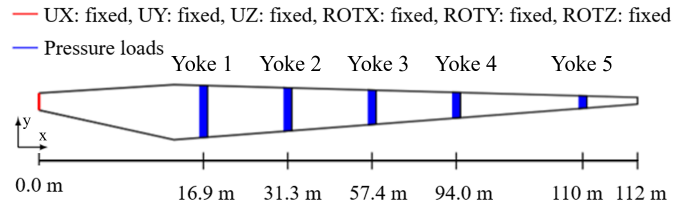


**Fig. 11** Boundary condition used for for modelling the simple yoke loading.

## 2.4 Creation of the solid model

To study the local effects and to capture the stresses through the blade thickness, a solid model was used. This was because shell elements cannot determine the stresses through the thickness accurately. To save computational energy, it was decided not to make a solid model of the entire blade, but only the part around the load introduction, 5 m long, using solid shell elements (SOLSH190).

For the creation of the solid model, the areas that defined the elements were first extruded to create volumes. These volumes were then meshed to have the same number of elements through the thickness everywhere in the model, ensuring that the meshes matched. Subsequently, the original layup was assigned to these elements as shown in Figure 12.

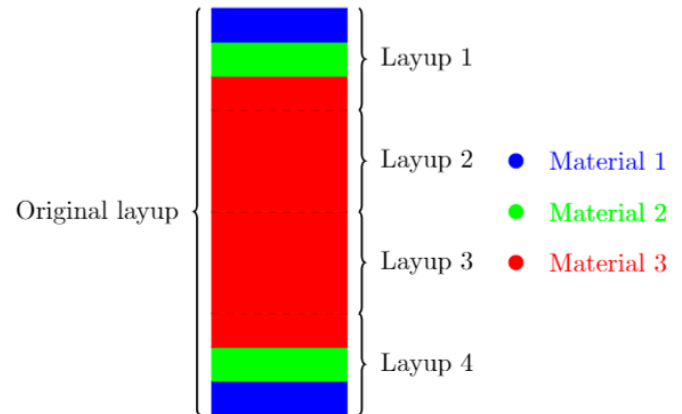


**Fig. 12** Creation of the layered solid model.

### 2.4.1 Validation of solid model

A simple model of the 5 m solid model was set up in order to validate it. The results was compared to the shell model. One end of the model was fixed while two load cases were considered, first a gravity load and then a spar cap load. The displacement vector sum for the gravity load case,  $9.81 \text{ m/s}^2$ , for the shell and solid model, showed a percentage difference of 4.6 %. However, the results are considered valid within the modelling choices that have been made.

Subsequently, a load of 100 kN was applied on the spar cap and the sum of displacement vectors is shown in Figure 13. Focusing on the distribution of displacements in the models, it was concluded that both models were similar as both experienced almost the same distribution. The biggest differences were found in the trailing edge panels, so the blade was not subsequently loaded in this region. Furthermore, based on the maximum values, the percentage difference found was 1 % and therefore it was assumed that the solid model worked correctly when the load was applied only at the spar cap.

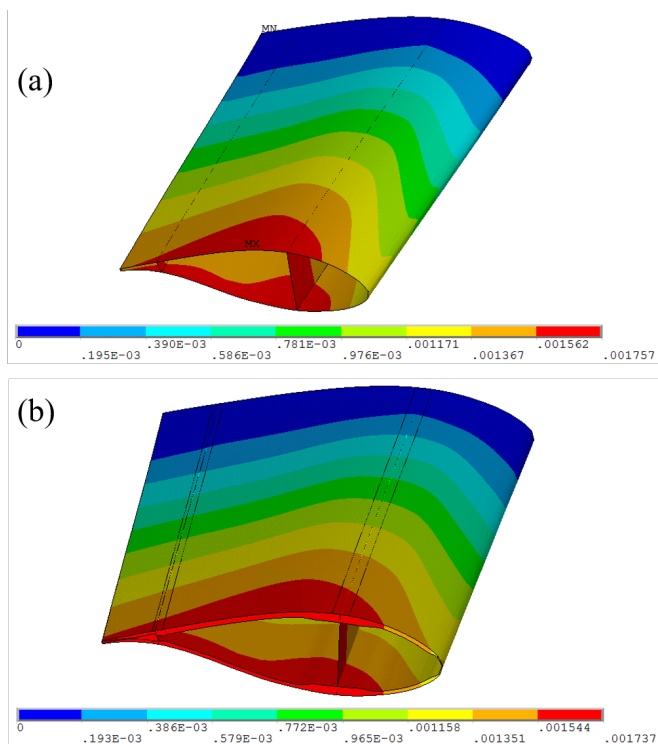


**Fig. 13** Displacement vector sum for the load in the spar cap case. (a) Shell model. (b) Solid model.

### 3. Results

#### 3.1 Full shell model with yokes

Yokes are designed for the positions shown in Figure 11 and they were based upon a reference design received from SGRE. The blade was in contact with two wooden blocks manufactured to follow the profile of the blade, with a set of I-beams surrounding them as shown in Figure 14. Rubber sheets were added at the interface to smooth over any surface imperfections on the wooden blocks and to spread the loads more evenly.

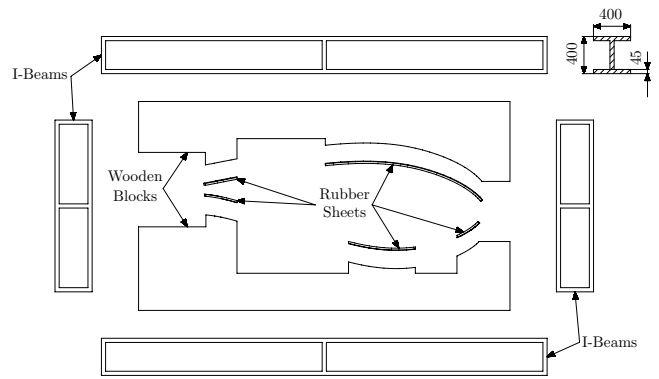


**Fig. 14** Design of yoke.

Figure 15 shows that the application the loads through the yokes instead of a pressure load decreased the deformation in the blade by a maximum of 4.9 %. This is assessed to be low enough to disregard any global stiffening effect in the blade due to the yokes.

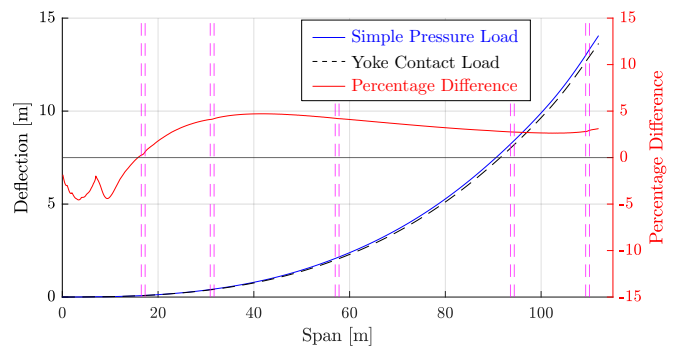


**Fig. 15** Simple pressure loading compared to loading through yokes.

#### 3.2 Local stresses in refined blade model

For this section, a shell-solid model with one yoke was used. The first shell region went from the root, i.e. 0 m, up to 55 m. Then, an MPC connection was used to connect it to the solid model, which extends until 60 m. Finally, a second MPC connection was used to connect it to the rest of the shell model until the tip at 112 m. This model will be referred to as the *shell-solid model* and it is shown in Figure 16 with the applied boundary conditions. The purpose of this model was to investigate the local effects around the load introduction including changes in displacements, stress distribution and failure criteria.

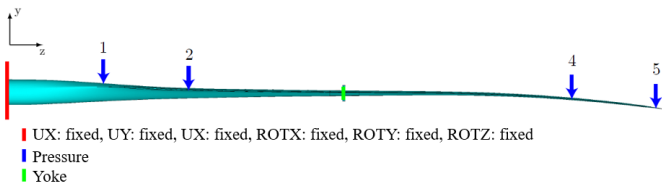


**Fig. 16** Shell-solid model with the yoke load case.

The results are shown in Figure 17 for the y-direction which is around the shell. The other directions gave the same overall picture but the x-direction, which is the direction along the blade length, had problems due to boundary effects where the solid model was connected to the shell.

The maximum compressive values were located in the MPC connections but those did not represent the real behaviour. In addition, some other compressive stresses were located where the yoke was positioned. These concentrations of stresses were due to the yoke contact in the trailing and leading edge panels. Therefore, a cutout was made to analyse it in detail, represented by a black line in Figure 17.

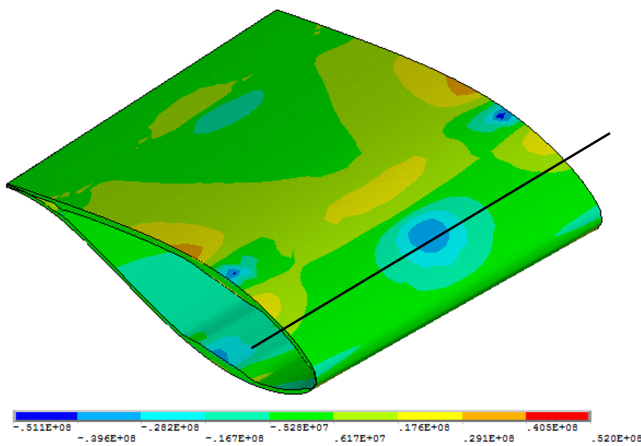


**Fig. 17** Stresses in the y-direction for the shell-solid model with the yoke load case, 56 m to 59 m.

The cutout is shown in Figure 18 and the distribution of the stresses is shown for Layer 5, which is the top layer consisting of biax glass fiber. The distance from the yoke to the neutral area, where the stresses are not affected by the yoke, was evaluated to be 650 mm. This distance is equal to 20 % of the chord length, considering this as 3.31 m.

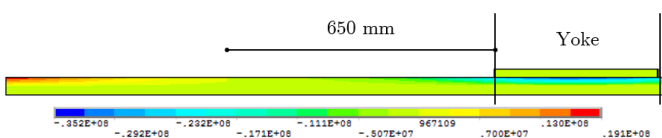


**Fig. 18** Stresses in the y-direction for the cutout in Layer 5.

### 3.2.1 Failure evaluation in refined blade model

The failure index is shown for the cutout in Figure 19. The highest failure index is in the top of layer 3 which is the balsa core of the sandwich structure. It can be seen that the failure index is distributed from the top to the bottom but it is not distributed significantly away from the yoke.

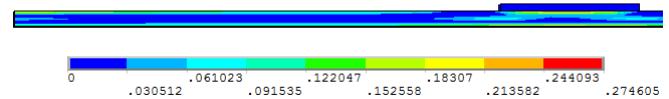


**Fig. 19** Failure evaluation in the cutout. The layers shown are the ones with the highest failure index.

### 3.3 Design study

An initial study was done on a simplified model to evaluate which parameters had the largest effect on the distribution of stresses due to the introduction of the yokes. It was assessed that the addition of a compliant material in between the contacting surfaces allowed a more uniform load distribution. In addition, changing the fraction of contact area had the largest effect on how the stresses were distributed.

A design study was then performed on the blade to evaluate these conclusions. The contacts were concentrated on the spar caps and the region around the shear web. Avoiding contact on the panels apart from these was observed to reduce the stress concentrations at the transitions between the spar cap and the panels. The addition of the rubber sheet was also beneficial, since the load was distributed much more evenly.

## 4. Discussion

### 4.1 Distance of local stresses

The evaluated influential distances for the local effects of the yoke are based on visual judgment and therefore they will have a high uncertainty. This is a problem since one of the primary goals of the project is to evaluate that distance. It would have been better to do a mathematical expression to compare the results from the shell model and the solid model in order to determine the neutral zone.

### 4.2 Geometrically nonlinear analysis

All the analyses should have been geometrically nonlinear in order to capture the effects of the large displacements. This is not done since it would result in problems with buckling even under the ideal load case. This is a problem because some of the load

cases cannot be solved due to excessive distortion of some of the elements. In the load cases that were able to solve, higher local stresses and deflections were observed due to local buckling in the blade. Since the aim of this project is to evaluate local effects of the load introduction, it is a problem if other local effects are introduced. Thus, it is chosen to do linear analyses instead.

The biggest issue with not doing the geometrically nonlinear analysis is that buckling behavior cannot be captured. This is a problem since the local load introduction might provoke some new buckling modes since the geometry of the blade will be changed at the load introduction. This imperfection will change the buckling load and possibly by a significant amount so buckling will occur, but this can neither be confirmed nor rejected. In order to investigate this, a new blade has to be designed with a higher stiffness in the problematic areas, which is necessary to be able to solve the nonlinear analysis.

#### **4.3 Deficits in refined blade model**

The solid model also has some problems as for example that the geometry is not the same as the shell model. This is due to the shell having uniform thickness and the overlapping definitions of the geometry in the shell model. This will change the stiffness and thereby also the displacement.

The element used is the solid shell element (SOLSH190) and it does not pass the patch test if the elements are distorted in the thickness direction. Therefore, it is not guaranteed that the solution will converge to the correct solution when the mesh is refined infinitely. This will only be a problem where the thickness changes and therefore, this is not a problem in the trailing edge panel but it will make a difference around the connection of the mini web and the transition to the spar cap.

The layup in the trailing and leading edge panels is a sandwich structure which consists of two facesheets, with glass fiber and a core of balsa wood. These materials have very dissimilar material properties thus, it is not recommended to use them within the same element. In the spar caps, the layup consists of glass fiber and carbon fiber which have more similar material properties, which decreases the problem here. Therefore, this problem is expected to have the highest impact in the trailing edge panels and the leading edge where the results will be too stiff.

#### **4.4 Connection between the shear web and the outer shell**

The connection between the spar cap and the outer shell is not modelled correctly too, since the actual connection is far more complex than what is modelled. Therefore, the results around this connection are not expected to be accurate. In the solid model, stresses due to tension in the thickness direction are seen, which might cause delamination in the spar cap. These stresses are due to the connection between the shear web and the spar cap not being modelled correctly and they do not represent the real stresses in that part. If those areas are to be investigated further, a more detailed model has to be created for that purpose.

Furthermore, due to this connection the results in the shear web will not be correct. In the ideal load case, all the forces are applied directly in the shear web and therefore the stresses will be too high. Consequently, the stresses in the shear web were not included in the analysis. This is not ideal, especially in the design study since the load is concentrated more around the shear web. Thus, it would have been necessary to evaluate the failure criteria here as well.

#### **4.5 Only one load direction**

Since only the flapwise positive load case has been considered, the conclusions do not necessarily agree if other load directions are investigated. This is expected to make the biggest difference for the design study since material is removed from the yoke in the leading edge. This is a major problem since this is the main load bearing area for the edgewise direction.

### **5. Conclusion**

The ideal moment curve provided by SGRE is approximated using B-splines to obtain the ideal load distribution. They are then condensed into discretized loads, which would act together to generate a moment response that is as close to the ideal moment curve as possible, for every load case. Due to the blade being too compliant it has not been possible to do a geometrical nonlinear analysis due to buckling.

An optimization problem is then defined to determine the best yoke positions along the blade that approximated the ideal moment curve as closely as possible. It is found that five yokes placed along the blade yielded the optimal solution and the force to be applied at each position are also determined. Simple pressure loads are

applied on the optimized loading points to compare the results against the ideal load distribution.

Yokes are designed for each of these loading points and used on the shell model to apply the optimized loads. The results from this model are compared to the results from the ideal load distribution and the simple pressure loads. It is assessed that neither of the approximations results in a significant global stiffening effect on the blade.

A 5 m part of the blade is created as a refined solid model in order to investigate the local effects due to yoke loading. Two approaches are considered, both of which use solid-shell elements (SOLSH190). The first approach creates a unique element for every layer through the thickness and uses MPCs to connect adjacent elements, since they do not share nodes. The second approach creates four elements in the thickness direction for the entire section under consideration and then uses layered solids to define the layup. The layered solids approach is found to provide closer results to the shell model and is therefore used for further analyses.

In order to evaluate the local effects due to the yoke loading, the created solid model section is implemented together with the shell model provided by SGRE. A yoke is connected to the solid part of the blade and the remaining four yoke loads is applied as a pressure. The model is then evaluated in terms of normal and shear stresses, as well as maximum failure criteria. From these analyses, it is possible to conclude that the effects from the load introduction extend for less than 75% of the chord length, but further investigation has to be made to get a more accurate number.

A simplified model is setup to evaluate the effect of changing different aspects of the yoke assembly on the stress distributions observed in the blade. Of all the variations attempted, it is observed that reducing the contact area between the yoke and the blade to concentrate around the stiffened regions of the blade over the spar-cap and the mini-web had the largest effect on the stress distributions.

In order to better evaluate the effect of the contact area has on the local effects a design study of two different yoke geometries is performed. One geometry which has contact over most of the blades surface and one which mainly has contact with the spar cap of the blade. The two cutouts is connected to the created refined solid part of the blade by contact elements and a force is applied

to the yokes. The normal stresses and failure index are evaluated.

Based on the design study of local effects study it can be concluded that concentrating the contact area over the spar caps reduces the stress concentrations in the panels without increasing the stresses in the spar cap by much. It cannot be concluded whether or not changing the contact area will change the spanwise distance of the local effects. Furthermore based on the initial studies using rubber distributes the load more evenly and thereby reduce stress concentrations.

### Acknowledgement

The authors of this work gratefully acknowledge Grundfos for sponsoring the 9<sup>th</sup> MechMan symposium.

### References

- [1] E. Hau, Wind Turbines: Fundamentals, Technologies, Application, Economics. Springer Berlin Heidelberg, 3rd ed., 2013.
- [2] T. Burton, E. Bossanyi, N. Jenkins, and D. Sharpe, Wind Energy Handbook. Chichester, West Sussex, U.K: John Wiley & Sons Ltd, 2nd ed., 2011.
- [3] L. Mishnaevsky, K. Branner, H. N. rgaard Petersen, J. Beauson, M. McGugan, and B. F. rensen, "Materials for wind turbine blades: An overview," Materials, vol. 10, no. 10:1285, 2017.
- [4] R. H. Barnes, E. V. Morozov, and K. Shankar, "Improved methodology for design of low wind speed specific wind turbine blades."
- [5] Dansk Standard, "Wind turbines - part 23: Full-scale structural testing of rotor blades," IEC 61400-23, 2014.